ОБЪЕДИНЕННЫЙ
ИНСТИТУТ
ЯДЕРНЫХ
ИССЛЕДОВАНИЙ
Дубна

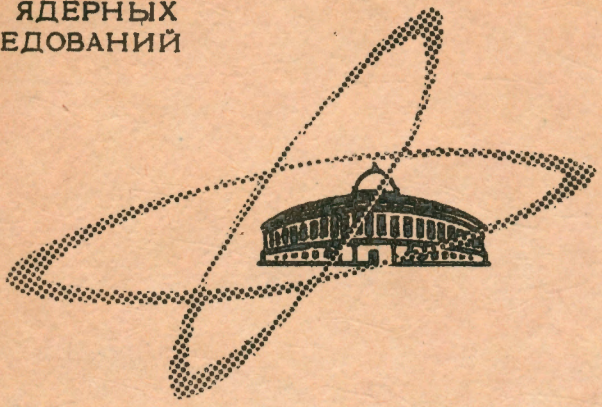

E2 - 3638

V.C.Suslenko, V.I.Kochkin

ЛАБОРАТОРИЯ ЯДЕРНЫХ ПРОБЛЕМ

ANALYSIS OF THE PERIPHERAL MODEL FOR THE PROCESS $p+p \rightarrow p+n+\pi^+$ AT 0.5 - 0.7 GeV

1967.

E2 - 3638

V.C.Suslenko, V.I.Kochkin

ANALYSIS OF THE PERIPHERAL MODEL FOR THE PROCESS $p+p \to p+n+\pi^+$ AT 0.5 - 0.7 GeV

Submitted to Nucl. Phys. and ЯФ

The concepts of the peripheral model (PM or OPEM)[1-3] for the single-pion production in the nucleon-nucleon collisions were verified by comparing with experimental data for the distributions of nucleons produced in the process

$$p + p \to p + n + \pi^{+} \qquad (1)$$

at incident proton energies T = 970, 2000 and 2850 MeV[2]. It was established that the experimental data can be explained on the basis of PM provided that the unknown function characterizing the pion-nucleon form-factor dependent on the value of the momentum transfer Δ^2 and independent of the incident energy T has the shape[2]

$$G(\Delta^2) = \frac{0.72}{1 + \frac{\Delta^2 + \mu^2}{4{,}73\,\mu^2}} + 0.028. \qquad (2)$$

Later it was shown that it is better to choose $G(\Delta^2)$ as follows[5,6]

$$G(\Delta^2) = \frac{8\mu^2}{\Delta^2 + 9\mu^2} \quad \text{or} \quad G(\Delta^2) = \frac{9\mu^2}{\Delta^2 + 10\mu^2}, \qquad (3)$$

which are nearly the same as (2) and give good agreement with experimental data at three various energies. This fact is considered as a proof of the applicability of the peripheral model concepts in the given energy region.

In the present paper the calculated pion energy spectra are compared on the basis of the peripheral model with the experimental π^+-meson energy spectra measured at different angles Θ_π^L at the incident energies T = 660 MeV and 556 MeV with the aim of clearing up the possibility to use the concepts of the peripheral model in this energy region.

1. Expression for π^+ Meson Distributions in the $\bar{p} + \bar{p} \to \bar{p} + \bar{n} + \pi^+$ Process

In the frame of the peripheral model process (1) is described by four Feynman pole diagrams of fig. 1. The expression for the differential cross section can be written as [2]

$$d\sigma = (2\pi)^{-5} \frac{1}{F} \frac{m^4}{2} \Sigma \, | M_{fi} |^2 \, \delta^4 (P_f - P_i) \frac{d^3 q \, d^3 q_1 \, d^3 q_2}{q_0 \, q_{10} \, q_{20}} \qquad (4)$$

and the energy distributions at the given angles are determined by the expression

$$\frac{d^2\sigma}{dq_0 \, d\Omega} = \frac{(2\pi)^{-5}}{F} \frac{m^4}{2} |\vec{q}| \int \Sigma \, | M_{fi} |^2 \delta^4 (P_f - P_i) \frac{d^3 q_1 \, d^3 q_2}{q_{10} \, q_{20}} \, . \qquad (5)$$

To calculate expression (5) it is necessary to carry out the six successive integrations four of which could be performed using the δ^4-function. As to the two remaining integrations, it is convenient to carry them out numerically with the help of the L_R-reference system (fig.2) suggested in ref. [7]. Leaving off the details of these derivations described in [7], we

represent here the final result for the point of the pion energy spectrum relating to the kinetic energy $T_\pi^L = q_0^L - \mu$ and the angle Θ_π^L in the lab. (L) system

$$\frac{d^2\sigma}{dq_0^L \, d\Omega^L} = \frac{(2\pi)^{-5}}{F} m^4 |\vec{q}^L| \int_A^B d\cos\beta_j \, \rho^R(q_{j0}, \cos\beta_j) \int_0^\pi d\phi_j \, | M_{fi}(q_{j0}, \cos\beta_j, \phi_j) |^2 , \qquad (6)$$

where $j = 1,2$,

$$q_{j0}^L = \frac{1}{2(R_0^2 - R^2 \cos^2\beta_j)} \{ R_0 (R_0^2 - R^2) + R\cos\beta_j \sqrt{[(R_0^2 - R^2)^2 - 4m^2 (R_0^2 - R^2 \cos^2\beta_j)]} \} , \qquad (7)$$

$$R_0 = p_{10}^L + m - q_0^L \, , \qquad (8)$$

$$R = | \sqrt{[(p_1^L)^2 + (q^L)^2 - 2 p_1^L q^L \cos\Theta_\pi^L]} | , \qquad (9)$$

$$\rho^R(q_{j0}, \cos\beta_j) = \left| \frac{(q_{j0}^L)^2 - m^2}{R_0 \sqrt{[(q_{j0}^L)^2 - m^2]} - q_{j0}^L R \cos\beta_j} \right| , \qquad (10)$$

$$A = (\cos\beta_j)_{\lim}^{low} = \left| \sqrt{\left[\frac{4m^2 R_0^2 - (R_0^2 - R^2)^2}{4m^2 R^2} \right]} \right| , \qquad (11)$$

$$B = (\cos\beta_j)^{up}_{lim} = \frac{1}{2m}\,\frac{(R_0^2 - R^2) - 2m^2A^2}{|\sqrt{[R_0^2 - (R_0^2 - m^2)A^2]}|}\,. \qquad (12)$$

It is convenient to write down the square of the whole matrix element relating to the four diagrams of fig. 1 of process (1) as follows

$$|M_{fi}|^2 = (2\pi)^2 \frac{G_r^2}{m^4}[(c_1^2 + c_3^2)X^2 + (c_2^2 + c_4^2)Y^2 + (c_1c_3 + c_2c_4)ZZ^*]\,, \qquad (13)$$

where $G_r^2 = \frac{16\pi m^2}{\mu^2} f^2$, $f = 0.28$ is the coupling constant of strong interaction, $(c_1^2 + c_3^2)X^2$, $(c_2^2 + c_4^2)Y^2$ are the sums of the square of the matrix elements of diagrams a), c) and b), d), respectively; $(c_1c_3 + c_2c_4)ZZ^*$ is the sum of the interference terms of the diagrams a), c) and b), d); $c_1, \ldots, c_4$ are the basic isospin coefficients corresponding to the diagrams a) – d), for which in the case of process (1) the following relation takes place

$$(c_1^2 + c_3^2) = (c_2^2 + c_4^2)^2 = (c_1c_3 + c_2c_4) = \frac{20}{9}\,. \qquad (14)$$

A detailed expression was obtained for the square of the peripheral matrix element (13) in ref.[2]. The calculation of the matrix element in the present study takes into account the specific feature of process (1) at the given energy, namely, the fact that in the energy region T = 500–700 MeV the main contribution to the amplitude of πN-scattering is due to the (3/2,3/2) resonance. It means that it is necessary to take into account the contribution from the amplitude with $\ell = 1$, $j = 3/2$ only. The virtuality of one of the pions in diagrams a), ..., d) was taken into account basing on the derivation of the one-dimentional dispersion relations obtained in ref.[8].

In the following formulae (15)–(32) the notations are the same as in ref.[2], where

$\frac{1}{t_1^2 + \mu^2}$ is the propagator function of the virtual pion,

$G(t_1^2) = K(t_1^2)\,K'(t_1^2)$ is the function depending on the momentum transfer t_1^2,

$K(t_1^2)$ is the pionic form-factor and

$K'(t_1^2)$ is the ratio of the whole propagator to the perturbative one,

$\sigma_{33}(u)$ is the (3/2 3/2) resonance total cross section of πN-scattering described by the phenomenological formula[9], $f_{1+}(u, t_1^2)$ is the (3/2 3/2) resonance amplitude of the virtual πN scattering, $\Gamma(t_1^2)$ is the factor taking into account the virtuality of one of the pions in the virtual πN scattering in diagrams of fig. 1 derived in ref.[8] on the basis of one-dimensional dispersion relations.

The above-mentioned suggestions adopted the values X^2, Y^2, ZZ^* in expression (13) have the following explicit forms

$$X^2 = u^2 t^2 \Pi^2(t_1^2)\,|f_{1+}(u, t^2)|^2 (1 + 3\cos^2\Theta^P)\,, \qquad (15)$$

$$Y^2 = u^2 \bar{t}^2 \Pi^2(\bar{t}_1^2)\,|f_{1+}(u, \bar{t}^2)|^2 (1 + 3\cos^2\epsilon^P)\,, \qquad (16)$$

$$ZZ^* = u^2 \Pi(t^2)\,\Pi(\bar{t}^2)\,|f_{1+}^*(u, t^2)\,f_{1+}(u, \bar{t}^2)|\,\times$$

$$\{(u + m)R_{(-)}[1 + 9\cos\Theta^P\cos\epsilon^P\cos\alpha^P - 3(\cos^2\Theta^P + \cos^2\epsilon^P)] +$$

$$(u - m)R_{(+)}[\cos\alpha^P + 3\cos\Theta^P\cos\epsilon^P]\}\,, \qquad (17)$$

where

$$H(t_i^2) = \frac{1}{t_i^2 + \mu^2} G(t_i^2), \qquad (t_i^2 = t^2, \bar{t}^2) \tag{18}$$

$$f_{1+}(u, t_i^2) = \frac{p_1^P}{q^P} \Gamma(t_i^2) \sqrt{\left[\frac{\sigma_{33}(u)}{8\pi}\right]}, \tag{19}$$

$$\Gamma(t_i^2) = \left(1 + \frac{t_i^2 + \mu^2}{4m^2}\right)^{1/2} \left[1 + \frac{3(t_i^2 + \mu^2)}{2m(u - m)}\right] \left[1 + \frac{t_i^2 + \mu^2}{2m(u - m)}\right]^{-3}, \tag{20}$$

$$\sigma_{33}(u) = \frac{2\pi}{(q^P)^2} \left[\frac{\gamma^2}{(u - u_0)^2 + \gamma^2/4}\right], \qquad \gamma = \left[\frac{2(q^P \cdot a)^3}{1 + (q^P \cdot a)^2}\right] \gamma_0, \tag{21}$$

$$R_{(+)} = [(p_{10}^P + m)(p_{20}^P + m)]^{1/2}, \qquad R_{(-)} = [(p_{10}^P - m)(p_{20}^P - m)]^{1/2}; \tag{22}$$

$$\cos\Theta^P = \frac{1}{2 q^P p_2^P} [\bar{r}^2 + (m^2 + \mu^2) - 2 q_0^P p_{20}^P], \tag{23}$$

$$\cos\epsilon^P = \frac{1}{2 q^P p_1^P} [r^2 + (m^2 + \mu^2) - 2 q_0^P p_{10}^P], \tag{24}$$

$$\cos\alpha^P = \frac{1}{2 p_1^P p_2^P} [2m^2 - W^2 + 2 p_{10}^P p_{20}^P], \tag{25}$$

$$q_0^P = \frac{1}{2u}(u^2 + \mu^2 - m^2), \qquad q^P = [(q_0^P)^2 - \mu^2]^{1/2} \tag{26}$$

$$p_{10}^P = \frac{1}{2u}(u^2 + m^2 + \bar{t}^2), \qquad p_1^P = [(p_{10}^P)^2 - m^2]^{1/2} \tag{27}$$

$$p_{20}^P = \frac{1}{2u}(u^2 + m^2 + t^2), \qquad p_2^P = [(p_{20}^P)^2 - m^2]^{1/2} \tag{28}$$

$$u^2 = W^2 - 3m^2 - t^2 - \bar{t}^2 \tag{29}$$

In expressions (22) - (28) the upper index "p" denotes the reference system where $\vec{q}^P + \vec{q}_2^P = 0$. As a result, the square of the matrix element $|M_{\pi\pi}|^2$ for pions (particle q), produced in process (1) turns out to be expressed through the invariants $W^2, r^2, \bar{r}^2, z^2, t^2, \bar{t}^2$, which are of equal strength to the fundamental set of the invariants $W^2, \omega^2, u^2, t^2, \Delta^2$. The invariants $W^2, r^2, \bar{r}^2, z^2$ can be simply expressed by the constant values determined in the L-system

$$r^2 = -(m - \mu)^2 + 2\mu T - 2T_\pi^L (m + T) - 2[T(T + 2m)]^{1/2} [T_\pi^L (T_\pi^L + 2\mu)]^{1/2} \cos\Theta_\pi^L, \tag{30}$$

$$\bar{r}^2 = -(m - \mu)^2 + 2m T_\pi^L, \qquad W^2 = 2m(2m + T), \tag{31}$$

$$z^2 = (q_{10}^L + q_{20}^L)^2 - (\vec{q}_1^L + \vec{q}_2^L)^2 = R_0^2 - R^2 = \tag{32}$$

$$= (2m-\mu)^2 + 2T(m-\mu) - 2T_\pi^L(2m+T) + 2[T(T+2m)]^{1/2}[T_\pi^L(T_\pi^L+2\mu)]^{1/2}\cos\Theta_\pi^L .$$

The square of the matrix element contains the functional dependence on the integration variables $\cos\beta_j$ and ϕ_j only in the invariants $t^2 = -(q_1 - p_1)^2$, $\bar{t}^2 = -(q_1 - p_2)^2$, their expressions being as follows:

i) if, taking into account δ-functions, the integrations in expression (5) were made by the use of the differentials d^3q_2 and d^3q_1, successively, then

$$t^2 = 2\{p_{10}^L q_{10}^L - m^2 - \frac{q^L}{R}[(q_{10}^L)^2 - m^2]^{1/2}[(\frac{R^2}{q^L} + p_1^L\cos\Theta_\pi^L - q^L)\cos\beta_1 + (p_1^L\sin\Theta_\pi^L)(1-\cos^2\beta_1)^{1/2}\cos\phi_1]\}, \quad (33)$$

$$\bar{t}^2 = 2(mq_{10}^L - m^2);$$

ii) and if the integrations were made in an inverse order, i.e. at first over d^3q_1 and then over d^3q_2, then

$$t^2 = 2\{-\frac{1}{2}(2m^2+\mu^2) + mq_0^L + (m-q_0^L)q_{20}^L + \frac{q^L}{R}[(q_{20}^L)^2 - m^2]^{1/2}[(p_1^L\cos\Theta_\pi^L - q^L)\cos\beta_2 + (p_1^L\sin\Theta_\pi^L)(1-\cos^2\beta_2)^{1/2}\cos\phi_2]\}, \quad (35)$$

$$\bar{t}^2 = 2\{-\frac{1}{2}(2m^2+\mu^2) + p_{10}^L q_{10}^L + p_1^L q^L\cos\Theta_\pi^L + (p_{10}^L - q_0^L)q_{20}^L - R[(q_{20}^L)^2 - m^2]^{1/2}\cos\beta_2\}. \quad (36)$$

The integration limits A and B ((11) and (12), respectively) for the variables $\cos\beta_j$ and ϕ_j in the cases i) and ii) are the same, this fact

being the consequence of the identity of particles q_1 and q_2 with respect to their kinematics ($m_1 = m_2 = m$ is the nucleon mass).

2. The Comparison with Experimental Data

The energy distributions of π^+-mesons, produced in process (1), can be deduced by the numerical integration over the variables $\cos\beta_j$ and ϕ_j of expression (6).

The values of kinetic energy T_π^L of the pion spectrum at the given angle Θ_π^L can lay in the region

$$0 \le T_\pi^L \le T_{\pi\,max}^L \quad (\Theta_\pi^L), \quad (37)$$

$$T_{\pi\,max}^L(\Theta_\pi^L) = \mu\left\{\frac{(\frac{m}{\mu})p_{20}^B q_{0\,max}^B + k^B\cos\Theta_\pi^L[(\frac{m}{\mu})^2(q_{0\,max}^B)^2 - (p_{20}^B)^2 + (k^B)^2\cos^2\Theta_\pi^L]^{1/2}}{(p_{20}^B)^2 - (k^B)^2\cos^2\Theta_\pi^L} - 1\right\} \quad (38)$$

$$p_{20}^B = \frac{W}{2}, \qquad k^B = (\frac{W^2}{4} - m^2)^{1/2}, \qquad q_{0\,max}^B = \frac{1}{2W}(W^2 - 4m^2 + \mu^2). \quad (39)$$

From the realness condition for (38) we get the condition of the existence of the limiting angle

$$p_{20}^B - (\frac{m}{\mu})q_{0\,max}^B > 0; \quad (40)$$

The direct calculation of (38) shows that it does not hold, this fact determining the possibility of the whole physical range of angles, e.g.

$$0 \leq \Theta_{\pi}^{L} \leq \pi , \qquad -1 \leq \cos \Theta_{\pi}^{L} \leq +1. \qquad (41)$$

In the present investigation the energy distributions of π^+-mesons produced in process (1) at various angles Θ_{π}^{L} at kinetic energies of incident protons T = 670, 657, 654 and 556 MeV were calculated using the computer.

The calculated normalized spectra of π^+-mesons in comparison with present day existing experimental data[12-16] are shown in figs. 3-10. In all the calculations for the (3/2) resonance of the physical πN-scattering the values[9,11] u_0 = 1235 MeV, γ_0 = 58 MeV, $a = 6.3 \cdot 10^{-3}$ MeV^{-1} were taken.

The function $G(t_1^2)$ was taken in the form[5]

$$G(t_1^2) = \frac{8\mu^2}{t_1^2 + 9\mu^2}. \qquad (42)$$

The energy spectra calculated with σ_{ss} = const. in expression (6) and the curves of the phase volume (expression (6) with $|M_{fi}|^2$ = const.) were also obtained. These calculations were made with the aim to clear up the role of the 33-resonance of the physical πN scattering and that of the phase volume. These results of the calculations have shown that the experimental data cannot be explained only by the behaviour of the phase volume and that the 33-resonance is of great importance.

The agreement of the theoretical spectra of π^+-mesons deduced on the basis of a peripheral model with the experimental energy spectra for the wide range of angles in the energy region T = 556 - 670 MeV is to be considered as a good one in the main part of the region of the continuous spectrum except the region near the limiting energy where due to the poor resolving power of the experimental arrangement in the experimental spectra there is the additional yield of π^+-mesons from the process $p + p \to d + \pi^+$.

All the calculations were carried out using electronic computers of the Joint Research Institute.

3. Discussion of Results

As has been shown in refs.[2-6], the concepts of the peripheral model can be used to explain the single-pion production process in nucleon-nucleon collisions at energies above 800 MeV. However, the results of ref.[7] cast doubt on the complete quantitative success of the peripheral model, since the computations based on the formulae of ref.[2] turned out to be in contradiction with the energy and momentum conservation laws. Nevertheless, one may hope that using the peripheral model it is possible to describe qualitatively process (1) and that the peripheral model concepts in the energy region below 800 MeV can be useful. Earlier it was usually considered that there exists a satisfactory explanation of process (1) on the basis of the Mandelstam "resonance" model[10] in which the main attention was paid to the effects of πN and NN interactions in the final state and the matrix elements were considered to be constant. The peripheral model has the advantageous feature in comparison with the Mandelstam model, especially because of the fact that in the peripheral model there exists the explicit method for deriving matrix elements and their dependence on the characteristic invariants is clearly established. It is natural to assume the applicability of peripheral model concepts to the energy region below 800 MeV and to try to prove it by comparing with pion spectra as the pions are just the produced particles. The results of the present study show that the pion spectra at two different energies, namely, T=556 and 660 MeV, can be qualitatively explained on the basis of the peripheral model using at these energies the same formfactor $G(t_1^2) = \frac{8\mu^2}{t_1^2 + 9\mu^2}$. This fact should be considered as a proof of the applicability of peripheral model concepts for process (1) in the energy region T = 500-700 MeV. Finally, we would like to mention that for the complete proof of the applicability of the peripheral model concepts it is desirable to calculate nucleon spectra taking into account the results of the ref.[7]. This problem will be the goal of our future investigation.

We are gratefully indebted to K.O. Oganesian, V.A. Yarba and Professors Z. Marić, V.P. Djelepov, L.I. Lapidus and S.V. Izmailov for their encouragements, support and useful discussions. One of us (V.C.S.) would like to

thank Profs. N.A. Perfilov and V.P. Djelepov for their kind permission to carry out this work at the Joint Institute for Nuclear Research, Dubna.

References

1. E. Ferrari, F. Selleri. Suppl. Nuovo Cim., 22, 453 (1962).
2. E. Ferrari, F. Selleri. Nuovo Cim., 27, 1450 (1963).
3. S.D. Drell. Rev . Mod. Phys., 33, 458 (1961).
4. J.D. Jackson. Rev. Mod. Phys., 37, 484 (1965).
5. F. Selleri. Nuovo Cim., 40, 236 (1965).
6. U. Amaldi, jr., R. Biancastelli and S. Francaviglia . Nuovo Cim., 47, 85 (1967).
7. V.C. Suslenko. Preprint P2-3597, Dubna, 1967.
8. E. Ferrari, F. Selleri. Nuovo Cim., 21, 1028 (1961).
9. M. Gell-Mann, K.M. Watson. Ann Rev. Nucl. Sci., 4, 219 (1954).
10. S. Mandelstam. Proc. Roy. Soc., 244, 491 (1958).
11. Da Prato. Nuovo Cim., 22, 123 (1961).
12 A.G. Meshkovsky, Ya. Shalamov, V.A. Shebanov. J. Expt. Theoret. Phys. 35, 64 (1958).
13. M.G. Mescheryakov, V.P. Zrelov, I.K. Vzorov, A.F. Shabudin . J. Expt. Theoret. Phys., 31, 45 (1956).
14. V.G. Vovchenko, G. Helfer, A.S. Kuznetsov, M.G. Mescheryakov, V. Sviatkovsky. J. Expt. Theoret. Phys., 39, 1557 (1960).
15. V.G. Vovchenko. Thesis, LFTI (1965), Doklady AN SSSR 163, 1348 (1965).
16. B.S. Neganov, O.V. Savchenko. J. Exptl. Theoret. Phys., 32, 1265 (1957).
17. A.G.Meshckovsky, Yu.S. Pligin, Ya.Ya. Shalamov, V.A. Shebanov. J. Expt. Theoret. Phys., 35, 64 (1958).

Received by Publishing Department
on December 25, 1967

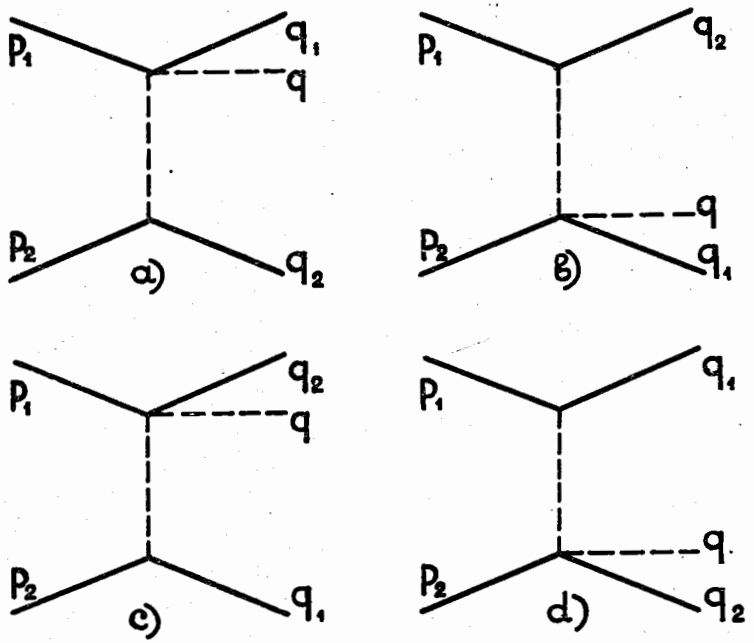

Fig.1. The four Feynman pole diagrams describing the process of single-pion production in the peripheral model.

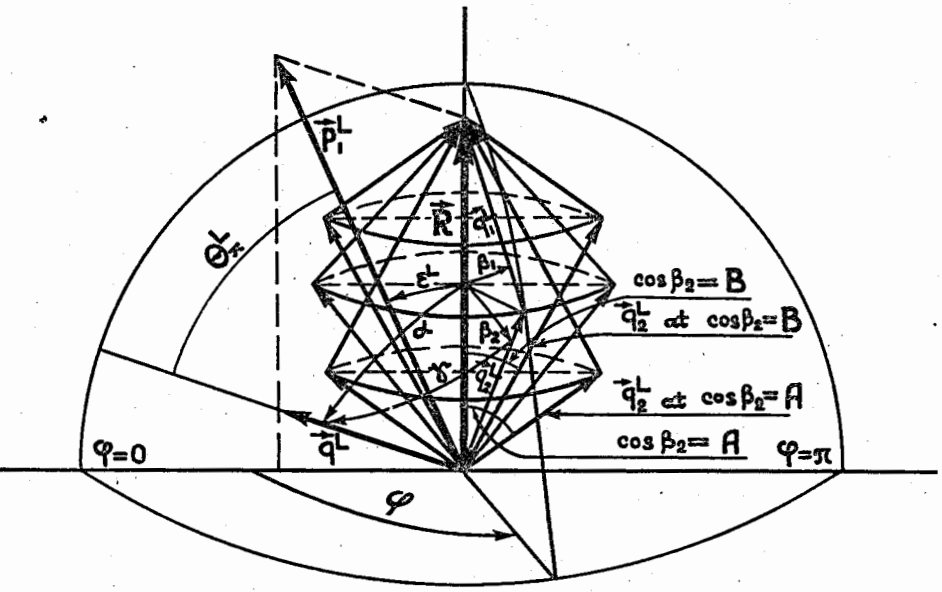

Fig.2. The positions of vectors and angles in the L_R -reference system ($\vec{R} = \vec{p}_1^L - \vec{q}^L$, the reference system rotated relative to the vector $\vec{p}_1^L$ by the angle ϵ^L , $\cos\epsilon^L = \frac{1}{R}(p_1^L - q^L \cos\Theta_\pi^L)$).

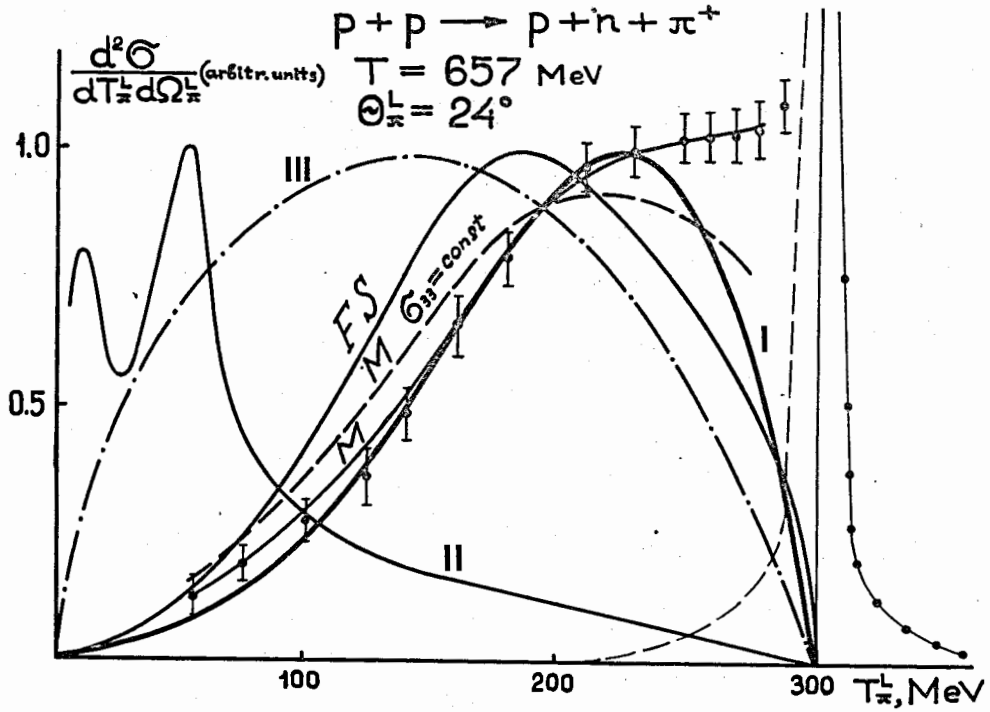

Fig.3. The comparison of experimental and theiretical laboratory kinetic energy π^+ -meson distribution at T = 657 MeV, $\Theta_\pi^L = 24°$ for the process $p + p \to p + n + \pi^+$. Thick full line | represents the result of calculation using formula (6) of the given paper.

Thin full line || is the result of the calculation of formula (6) with σ_{33} = const.

Dash-dotted line ||| represents the phase-volume curve (formula (6) with $|M_{fi}|^2$ = const).

The line labelled FS is the result of calculation using formula (3.87) of ref.[2].

Here for comparison the results of Mandelstam's theory (ref.[10]) are also represented (lines labelled by M). -experimental. data of ref.[13].

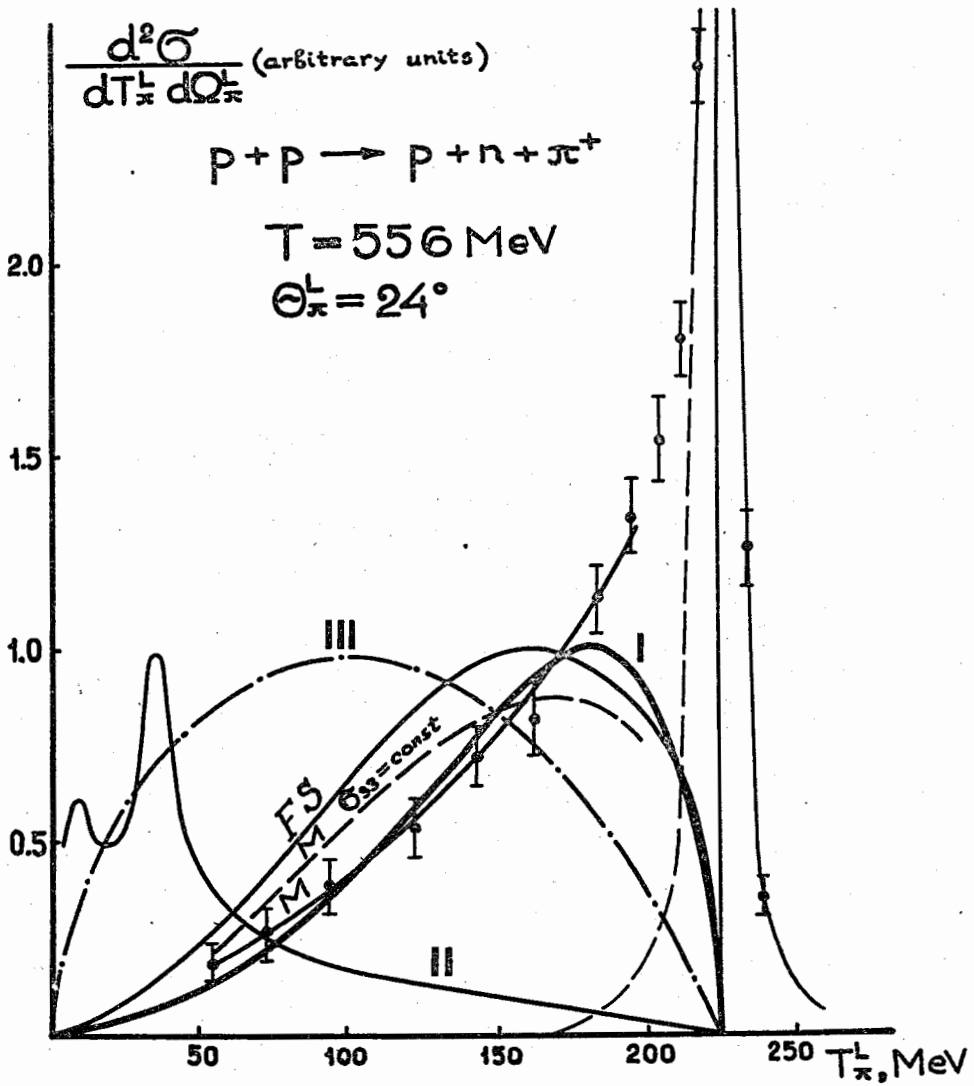

Fig.4. The same distribution and theoretical results as in Fig.3 at T= 556 MeV, $\Theta_\pi^L = 24°$. ⊕ -experimental data of ref./13/.

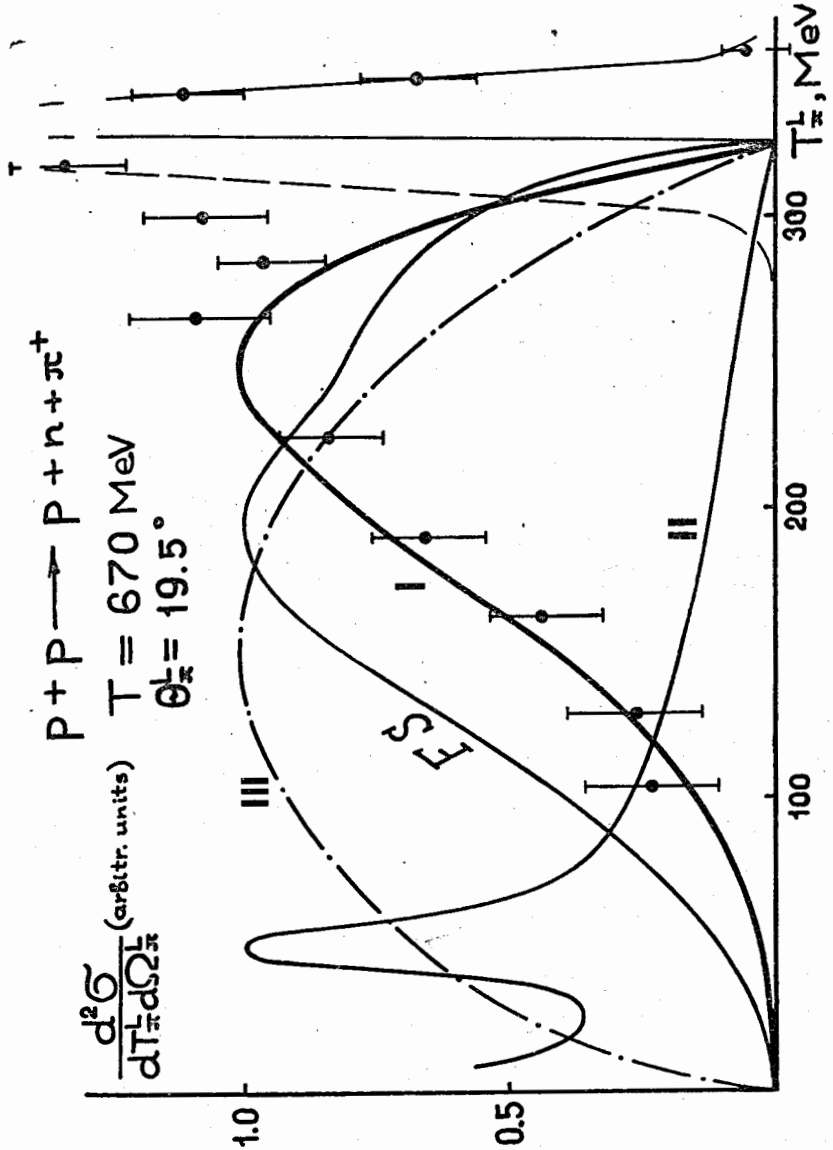

Fig.5. The same distribution and theoretical results (lines I, II, III and FS) as in Fig.3 at T = 670 MeV, Θ_π^L = 19.5°. ⊕ -experimental data of ref./12/.

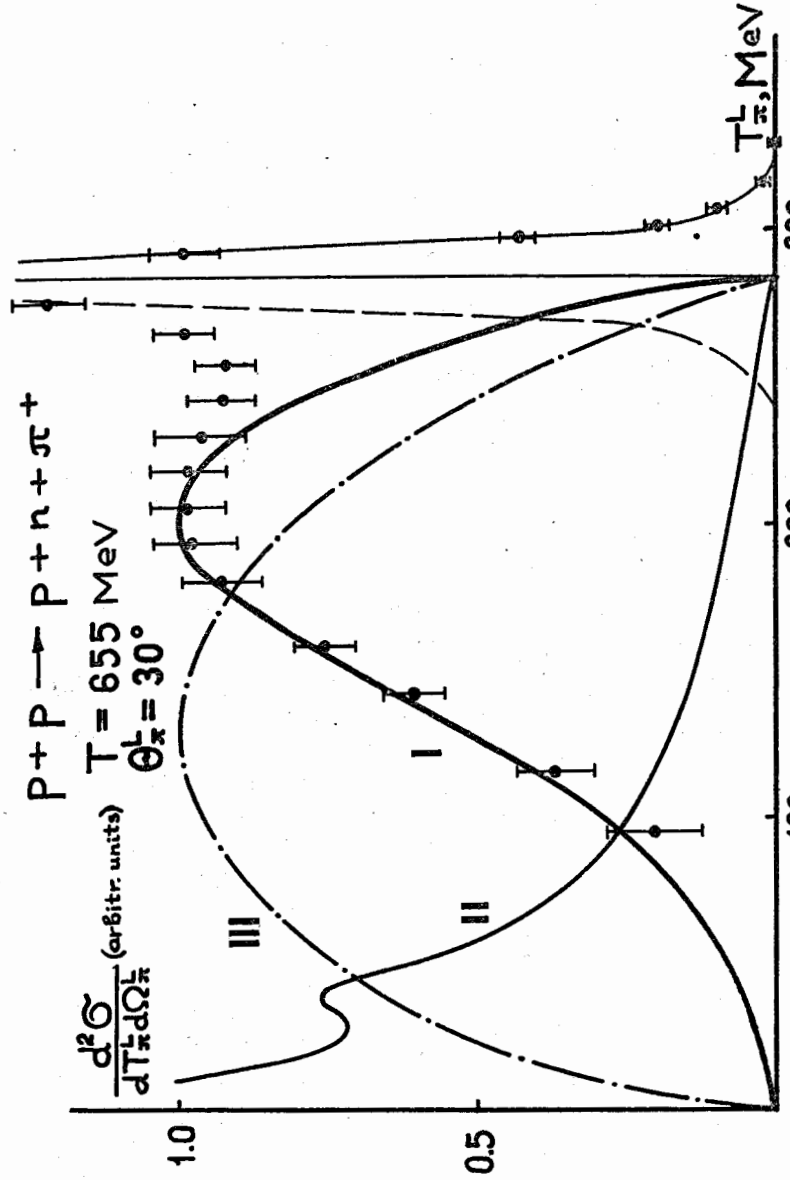

Fig.6. The same distribution and theoretical results (lines I, II and III) as in Fig.3 at T = 655 MeV, $\theta_\pi^L = 30°$.
I - experimental data of ref./15/.

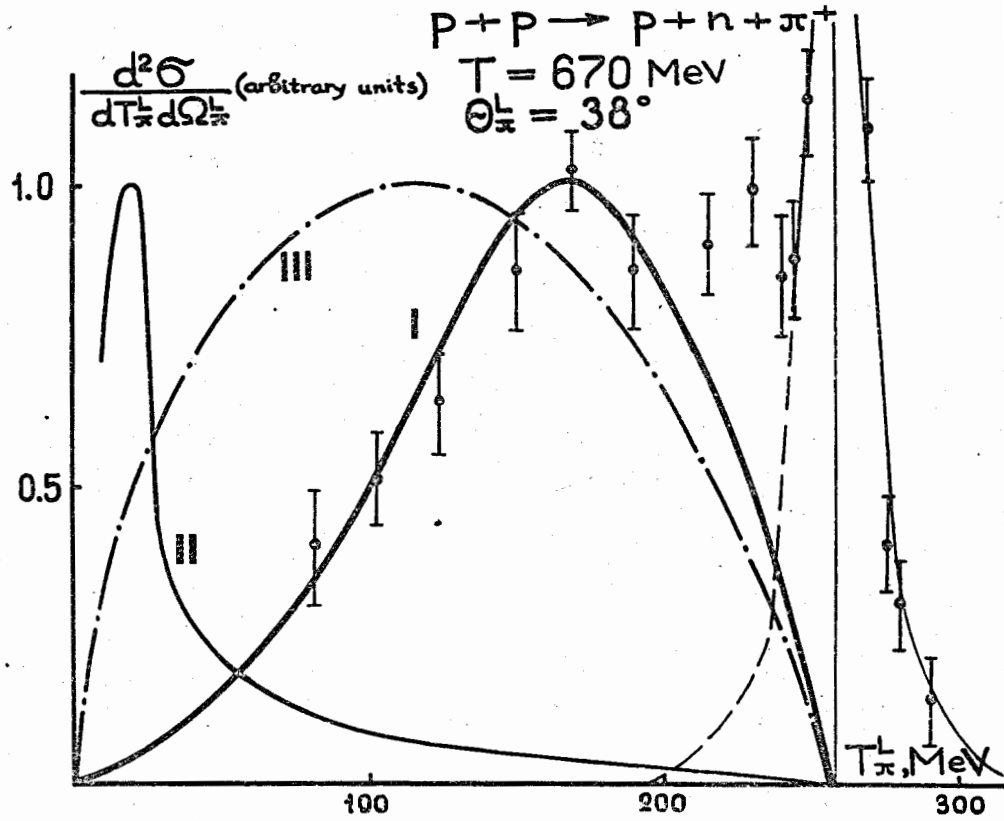

Fig.7. The same distribution and theoretical results (lines I, II and III) as in Fig. 3 at T = 670 MeV, $\theta_\pi^L = 38°$.
I - experimental data of ref./12/.

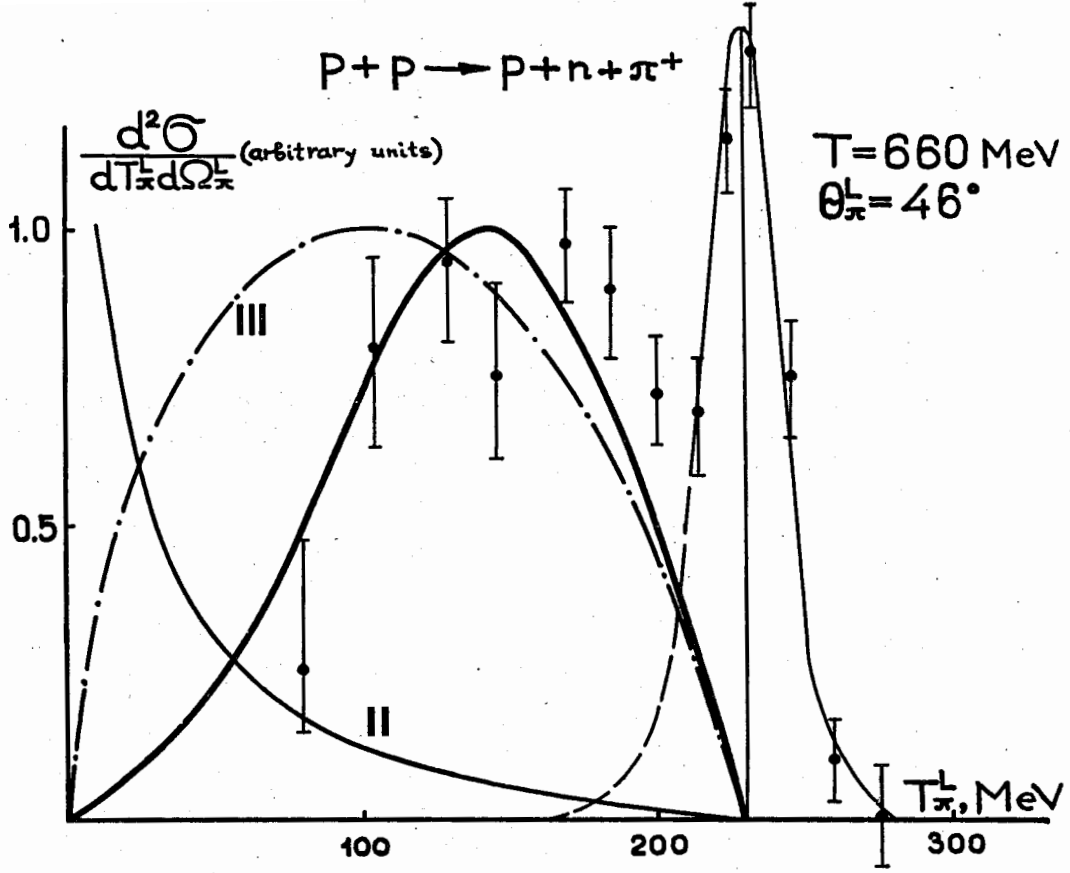

Fig.8. The same distribution and theoretical results (lines I, II and III) as in Fig.3 at T = 660 MeV, $\theta_\pi^L = 46^\circ$.
● - experimental data of ref. /17/.

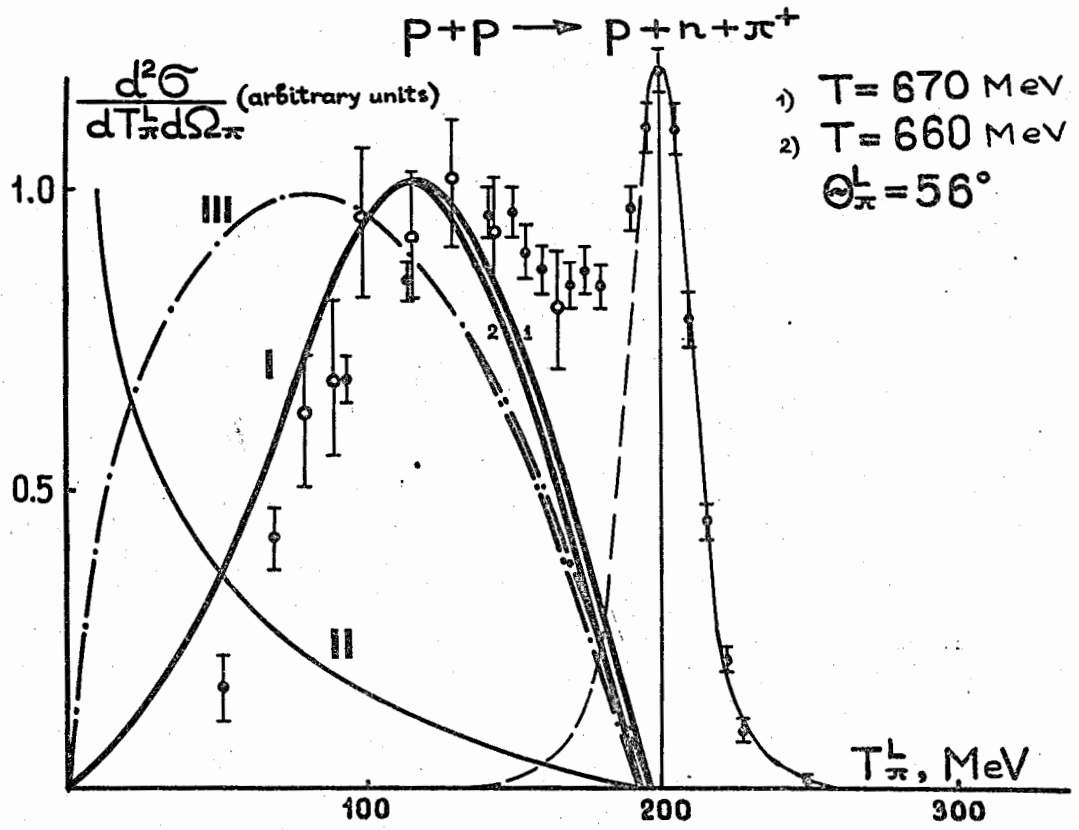

Fig.9. The same distribution and theoretical results (lines I, II and III) as in Fig.3 at T = 660 MeV, $\theta_\pi^L = 56^\circ$.
⊖ - experimental data of ref. /12/.
⊖ - experimental data of ref. /14/.

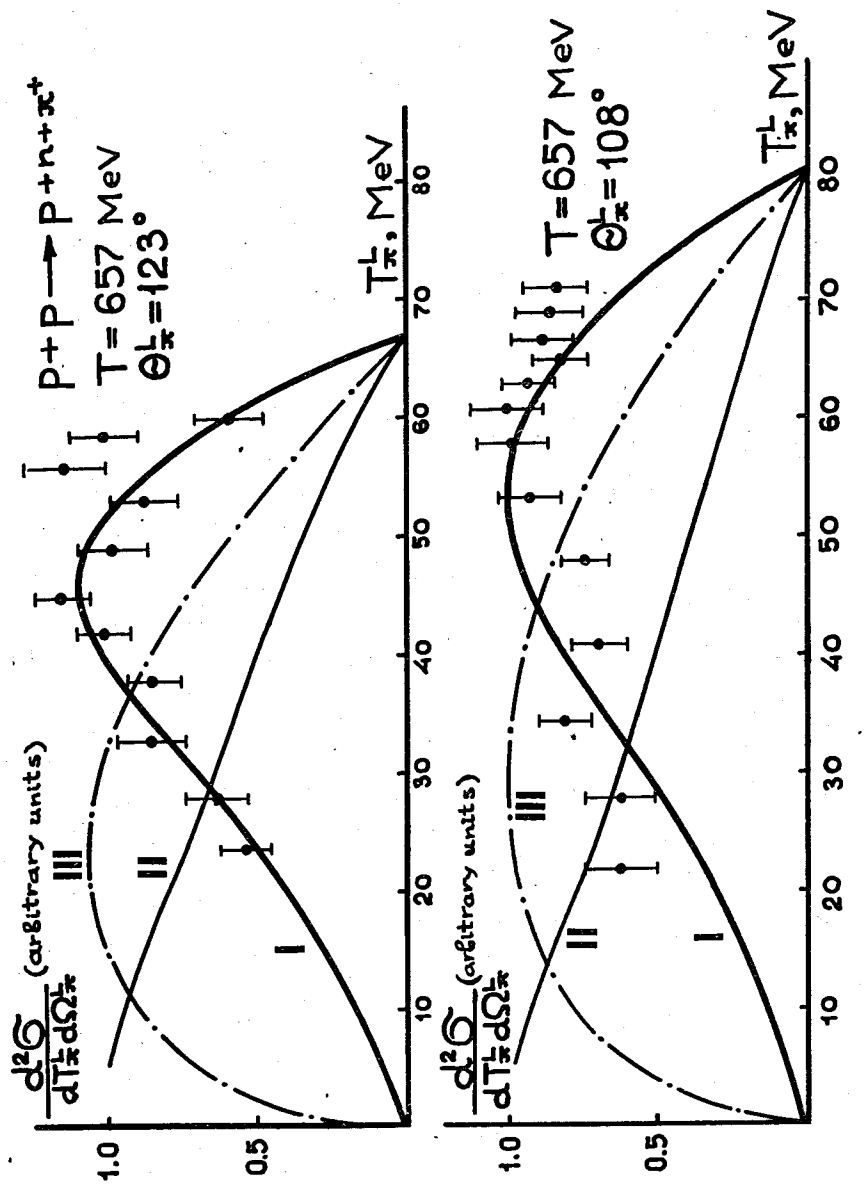

Fig.10(part 1).
The same distributions and theoretical results (lines I, II and III) as in Fig.3 at T= 657 MeV, Θ^L_π= 108°, 123°, 140° and 160°.
-experimental data of ref./16/.

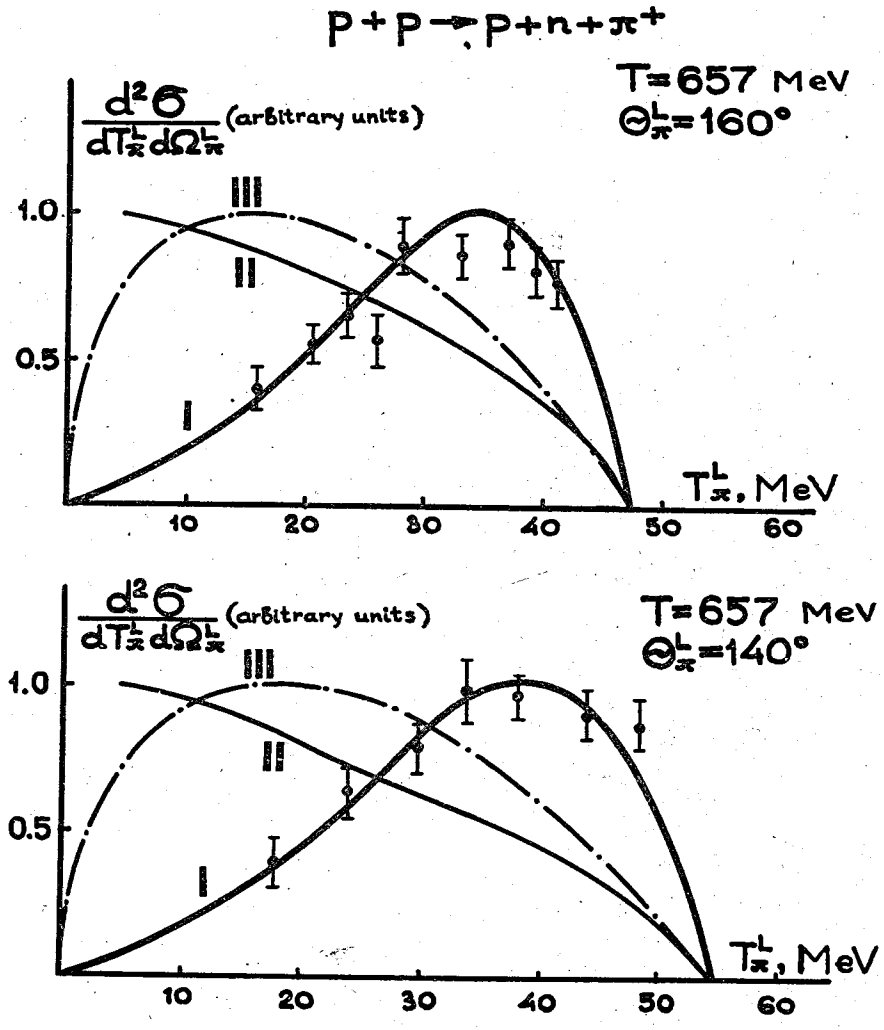

Fig.10(part 2).
The same distributions and theoretical results (lines I, II and III) as in Fig. 3 at T= 657 MeV, Θ^L_π= 108°, 123°, 140° and 160°.
-experimental data of ref./16/.